Approximate Sparse Stochastic Control for Time-Varying Systems with Control-Dependent Diffusion

Yong Wang[1], Haopeng Deng[2], Zhu Luo[3], and Lingyue Li[1]

***Abstract*—This paper proposes a scalable framework for sparse stochastic optimal control in time-varying systems with control-dependent diffusion. By relaxing the classical stochastic normality condition, we establish an approximate equivalence between ℓ_0 and ℓ_1 optimal control formulations under local or probabilistic regularity. The framework unifies sparsity, stochasticity, and safety by incorporating variational inequalities to handle state and control constraints. To overcome the curse of dimensionality, we develop efficient numerical solvers based on sparse grids, Tensor-Train decomposition, and neural residual networks. Numerical experiments on robotic and energy systems demonstrate substantial gains in control sparsity, safety compliance, and computational scalability, confirming the practicality and robustness of the proposed approach in high-dimensional, safety-critical settings.**

***Index Terms*—Sparse control, stochastic optimal control, probabilistic normality, high-dimensional solvers, HJB variational inequality**

I. Introduction

Sparse optimal control aims to reduce actuator usage and energy consumption by promoting inactivity in control signals, typically through ℓ_0-type regularization. This paradigm has proven effective in diverse applications such as energy management [1], actuator scheduling [2], and communication-constrained systems. In deterministic settings, ℓ_0-optimal strategies often exhibit bang-off-bang structures, and under suitable structural conditions, can be exactly recovered via convex ℓ_1 relaxations.

Extending these sparsity principles to stochastic systems introduces significant analytical and computational challenges. The associated value function satisfies a second-order, fully nonlinear Hamilton–Jacobi–Bellman (HJB) equation, where nonsmooth running costs and control-dependent diffusion prevent the application of standard tools such as dynamic programming and viscosity solution theory [3]–[5]. In particular, control-dependent noise disrupts the monotonicity conditions essential for solution comparison and uniqueness.

Recent works have addressed sparse stochastic control under simplified conditions. For instance, Ito *et al.* [6] and Mai and Yin [7] studied sparse control in linear systems with additive noise, while Luo and Wang [8] extended the theory to nonlinear systems with control-modulated diffusion by introducing a *stochastic normality condition* ensuring ℓ_0–ℓ_1 equivalence. However, this condition imposes global regularity requirements that are often violated in real-world systems—particularly those where actuation intrinsically modulates uncertainty, such as robotic manipulators and energy storage networks.

To overcome these limitations, this paper introduces a *relaxed stochastic normality framework* that permits local or probabilistic violations of classical assumptions. This generalization preserves the approximate equivalence between ℓ_0 and ℓ_1 formulations with high probability, even in the presence of control-dependent noise. As such, it significantly expands the applicability of sparse stochastic control to complex, safety-critical systems, as structured in Figure 1.

Beyond this theoretical advancement, we address two core challenges for practical deployment: the curse of dimensionality and the enforcement of hard state and input constraints [9]. To this end, we develop scalable solvers based on sparse grids, tensor-train (TT) decomposition, and neural Galerkin residual networks, enabling efficient computation in high-dimensional settings. Moreover, we formulate the control problem under a variational inequality framework that integrates sparsity, stochasticity, and constraint satisfaction in a unified manner.

The main contributions of this work are as follows:

1) We propose a unified theoretical framework for sparse stochastic control, grounded in viscosity solutions, backward SDEs, and a relaxed stochastic normality condition that enables approximate ℓ_0–ℓ_1 equivalence.
2) We develop scalable solvers for high-dimensional HJB equations, combining adaptive sparse grids, tensor-train decomposition, and neural residual correction.
3) We validate the methods on robotic and energy systems, demonstrating significant improvements in sparsity, safety, and computational efficiency under uncertainty.

II. Problem Formulation

A. Stochastic System Model and Assumptions

We consider the controlled stochastic differential equation (SDE)

$$\mathrm{d}x(t) = b\big(t, x(t), u(t)\big)\,\mathrm{d}t + \sigma\big(t, x(t), u(t)\big)\,\mathrm{d}W(t), \quad t \in [0, T], \tag{1}$$

with initial condition $x(0) = x_0 \in \mathbb{R}^n$, where:

Manuscript received May 2025.

[1]School of Arts and Sciences, Guangzhou Maritime University, Guangzhou 510725, China (emails: wyong9677@gmail.com; lilingyue@gzmtu.edu.cn).

[2]School of Intelligent Transportation and Engineering, Guangzhou Maritime University, Guangzhou 510725, China (email: qianyhp@gmail.com).

[3]Guangdong Communication Polytechnic, Guangzhou, China (email: abrity@gdcp.edu.cn). Lingyue Li is the corresponding author.

This work was supported by the National Natural Science Foundation of China under Grant 42301338.

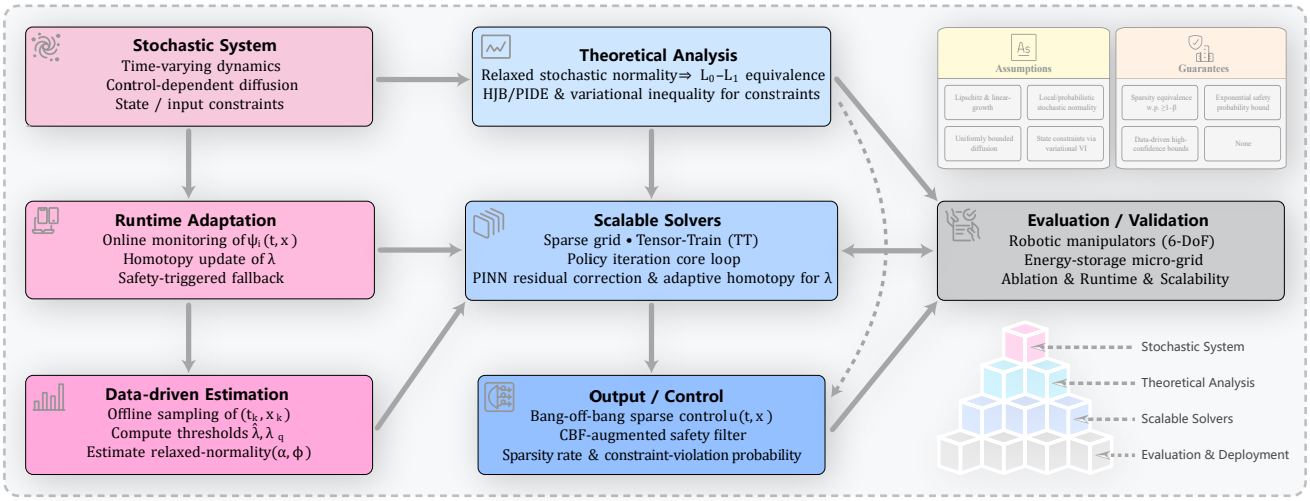

Fig. 1. Framework overview of sparse stochastic optimal control with control-dependent diffusion.

- $x(t) \in \mathbb{R}^n$ is the state;
- $u(t) \in U \subseteq \mathbb{R}^m$ is the control input, with U compact and convex;
- $W(t)$ is an r-dimensional standard Brownian motion on a filtered probability space $(\Omega, \mathcal{F}, \{\mathcal{F}_t\}, P)$;
- $b : [0,T]\times\mathbb{R}^n\times U \to \mathbb{R}^n$ and $\sigma : [0,T]\times\mathbb{R}^n\times U \to \mathbb{R}^{n\times r}$ are measurable functions.

We impose the following standard conditions [3]–[5].

Assumption 1: There exist constants $L, K > 0$ such that for all $t \in [0,T]$, $x, y \in \mathbb{R}^n$, and $u, v \in U$:

(i) (*Lipschitz continuity*)

$$\|b(t,x,u) - b(t,y,v)\| + \|\sigma(t,x,u) - \sigma(t,y,v)\| \le L\left(\|x-y\| + \|u-v\|\right).$$

(ii) (*Linear growth*)

$$\|b(t,x,u)\| + \|\sigma(t,x,u)\| \le K\left(1 + \|x\| + \|u\|\right).$$

(iii) (*Uniform boundedness in diffusion*)

$$\|\sigma(t,x,u)\| \le K, \quad \forall (t,x,u).$$

Remark 1 (Existence and uniqueness): Under Assumption 1, for any admissible control, SDE (1) admits a unique strong solution in $\mathcal{S}^2$, the space of square-integrable, adapted processes [5]. Furthermore, the dynamic programming principle and viscosity solution theory are applicable. See also [5, Theorem 5.2.1] for a formal proof of well-posedness.

The admissible control set is defined by:

$$\mathcal{U}[0,T] = \Big\{ u : [0,T]\times\Omega \to U \;\Big|\; u \text{ is } \{\mathcal{F}_t\}\text{-adapted}, \; \mathbb{E}\int_0^T \|u(t)\|^2\,\mathrm{d}t < \infty \Big\}.$$

B. Sparse Control Objective and Relaxation

We define the instantaneous sparsity measures:

$$\|u(t)\|_0 = \sum_{i=1}^m \mathbf{1}_{\{u_i(t)\neq 0\}}, \quad \|u(t)\|_1 = \sum_{i=1}^m |u_i(t)|.$$

The original sparse control problem aims to minimize the cost functional

$$J_0(u(\cdot)) = \mathbb{E}\left[\int_0^T \left(h(t,x(t)) + \|u(t)\|_0\right)\mathrm{d}t + g(x(T))\right], \tag{2}$$

where $h : [0,T]\times\mathbb{R}^n \to \mathbb{R}_+$ and $g : \mathbb{R}^n \to \mathbb{R}_+$ are continuous and Lipschitz continuous in x.

To enable tractable optimization, we relax the cost via ℓ_1 regularization:

$$J^\lambda(u(\cdot)) = \mathbb{E}\left[\int_0^T \left(h(t,x(t)) + \lambda\,\|u(t)\|_1\right)\mathrm{d}t + g(x(T))\right], \tag{3}$$

where $\lambda > 0$ is a tunable parameter promoting control sparsity.

C. HJB Equation and Value Function

The relaxed control problem admits the value function

$$V^\lambda(t,x) = \inf_{u(\cdot)\in\mathcal{U}[t,T]} \mathbb{E}_{t,x}\left[J^\lambda(u(\cdot))\right], \tag{4}$$

where the conditional expectation is taken given $x(t) = x$.

Under Assumption 1, standard results from stochastic control theory [3], [5] ensure that V^λ is the unique bounded, continuous viscosity solution of the following Hamilton–Jacobi–Bellman (HJB) equation:

$$\begin{aligned} &-\partial_t V^\lambda(t,x) - \inf_{u\in U}\left\{\mathcal{L}^u V^\lambda(t,x) + h(t,x) + \lambda\,\|u\|_1\right\} = 0, \\ &V^\lambda(T,x) = g(x), \end{aligned} \tag{5}$$

where the controlled second-order operator is

$$\mathcal{L}^u V(t,x) = b(t,x,u)^\top \nabla_x V(t,x) + \tfrac{1}{2}\,\mathrm{tr}\left(\sigma(t,x,u)\sigma(t,x,u)^\top \nabla^2_{xx} V(t,x)\right).$$

D. State Constraints via Variational Inequalities

To enforce state constraints, we consider a general (possibly non-convex) admissible set:

$$X = \bigcap_{j=1}^J \left\{x \in \mathbb{R}^n \mid \varphi_j(x) \le 0\right\}, \tag{6}$$

where each φ_j is locally Lipschitz continuous. Assume there exists a Lipschitz continuous penalty function Ψ satisfying

$$\Psi(x) \geq g(x) + c_0, \quad \forall x \in \partial X, \quad c_0 > 0. \tag{7}$$

Then the constrained value function satisfies the following multi-obstacle variational inequality:

$$\begin{aligned} \min\Big\{ &- \partial_t V^\lambda - \inf_{u\in U} \left(\mathcal{L}^u V^\lambda + h + \lambda\|u\|_1\right), \\ &\max_{1\leq j\leq J} \left\{\varphi_j(x),\ V^\lambda - \Psi(x)\right\} \Big\} = 0. \end{aligned} \tag{8}$$

Remark 2 (Numerical implementation): For sparse grid or tensor-train (TT) based solvers:

- Evaluate $\phi(x) := \max_j \varphi_j(x)$ at each node and apply obstacle projection;
- For stiff constraints or sharp domain boundaries, use a smoothed penalty of the form

$$\tilde{\Psi}(x) = \Psi(x) + \sum_{j=1}^{J} \eta_j \left[\varphi_j(x)\right]_+, \quad [\cdot]_+ := \max\{0, \cdot\},$$

to enhance numerical stability.

E. Extension to Lévy Jump-Diffusion Models

To model impulsive and heavy-tailed disturbances, we extend the stochastic system (1) to a Lévy jump–diffusion form:

$$\begin{aligned} \mathrm{d}x(t) = b(t,x,u)\,\mathrm{d}t + \sigma(t,x,u)\,\mathrm{d}W(t) \\ + \int_{\mathbb{R}^r\setminus\{0\}} \kappa(t,x^-,u,z)\,\widetilde{N}(\mathrm{d}z,\mathrm{d}t), \end{aligned} \tag{9}$$

where $\widetilde{N}$ is the compensated Poisson random measure associated with the Lévy measure ν, which satisfies the integrability conditions:

$$\int_{\|z\|>1} \nu(\mathrm{d}z) < \infty, \quad \int_{\|z\|\leq 1} \|z\|^p \nu(\mathrm{d}z) < \infty, \quad p \in (0,2). \tag{10}$$

The system remains well-posed under the following regularity assumptions.

Assumption 2 (Lipschitz and Linear Growth under Lévy Noise): There exist constants $L, K > 0$ such that for all (t,x,u,z):

$$\begin{aligned} &\|b(t,x,u) - b(t,y,v)\| + \|\sigma(t,x,u) - \sigma(t,y,v)\| \\ &\quad + \|\kappa(t,x,u,z) - \kappa(t,y,v,z)\| \leq L\left(\|x-y\| + \|u-v\|\right), \\ &\|b(t,x,u)\| + \|\sigma(t,x,u)\| \leq K(1 + \|x\| + \|u\|), \\ &\|\kappa(t,x,u,z)\| \leq K \cdot \min\{\|z\|, 1\}. \end{aligned}$$

Under conditions (10) and Assumption 2, the jump–diffusion SDE (9) admits a unique strong solution in $\mathcal{S}^2$, and the dynamic programming principle remains valid; see [10].

III. Sparse Stochastic Control via ℓ_1 Relaxation

This section develops the core theory of sparse stochastic control via ℓ_1-relaxation, including exactness results, practical threshold selection, robustness under model uncertainty, and extensions to jump-diffusion systems.

A. Exactness of ℓ_1 Relaxation

We begin with the main result showing that the ℓ_1-relaxed formulation recovers the ℓ_0-optimal control structure under relaxed stochastic normality.

Theorem 1 (Data-Driven Sparsity Equivalence with High Probability): Let $V^\lambda(t,x)$ be a differentiable approximation of the relaxed value function. Define the switching function:

$$\psi_i(t,x) := b_i^\top(t,x)\nabla_x V^\lambda(t,x) + \tfrac{1}{2}\mathrm{tr}\left[\sigma_i\sigma_i^\top \nabla^2_{xx} V^\lambda(t,x)\right]. \tag{11}$$

Let $\{(t_k,x_k)\}_{k=1}^N$ be sampled points. Define the empirical $(1-\rho)$-quantile and safety margin:

$$Q^{(i)}_{1-\rho} := \inf\left\{ q \mid \frac{1}{N}\sum_{k=1}^{N} \mathbb{I}\{|\psi_i(t_k,x_k)| \leq q\} \geq 1-\rho \right\}, \tag{12}$$

$$\Delta_{\mathrm{saf}} := \sqrt{\frac{\log(2/\beta)}{2N}}, \quad \lambda := \max_i \left(Q^{(i)}_{1-\rho} + \Delta_{\mathrm{saf}}\right). \tag{13}$$

Then, with probability at least $1-\beta$, the ℓ_1-optimal control

$$u_i^\lambda(t,x) = \arg\max_{u_i\in[-U_i^-, U_i^+]} \left(\psi_i(t,x)\,u_i - \lambda\,|u_i|\right) \tag{14}$$

exhibits a bang-off-bang structure and coincides with the ℓ_0-optimal control at no fewer than $(1-\rho)N$ of the sample points.

Rather than relying on global bounds of $\psi_i(t,x)$, we estimate thresholds via offline-sampled trajectories. For any user-specified risk tolerance (ρ,β), Theorem 1 ensures that a data-driven threshold λ yields bang-off-bang sparsity with high probability. In low-noise regimes, omitting the second-order term in (11) can still yield accurate switching decisions. This approach enables scalable implementation via the solvers described in Section IV.

B. Computable Lower Bound for λ^*

Although Theorem 1 ensures sparsity for any $\lambda \geq \lambda^*$, computing λ^* analytically is generally intractable. We instead propose a data-driven upper bound $\widehat{\lambda}$ with statistical guarantees.

Proposition 1 (Sample-Based Lower Bound for λ^*): Let $\{(t_k,x_k)\}_{k=1}^N$ be a set of offline-sampled time–state pairs, and define

$$\widehat{\lambda} := \max_{1\leq k\leq N} \max_{1\leq i\leq m} |\psi_i(t_k,x_k)| + \sqrt{\frac{\log(2/\beta)}{2N}}. \tag{15}$$

Then, with probability at least $1-\beta$, we have $\lambda^* \leq \widehat{\lambda}$, and for any $\lambda \geq \widehat{\lambda}$, the ℓ_1-optimal control (14) exhibits bang-off-bang sparsity as in Theorem 1.

Proof. Define $X_{k,i} := |\psi_i(t_k,x_k)|$ and let $\lambda^* := \sup_{t,x,i} |\psi_i(t,x)|$. Applying the Dvoretzky–Kiefer–Wolfowitz inequality [11], [12] to the empirical maximum yields, with probability at least $1-\beta$, the bound $\lambda^* \leq \widehat{\lambda}$. ∎

Implementation guideline.:

1) Sample N pairs (t_k,x_k);
2) Evaluate $\psi_i(t_k,x_k)$ via (11);
3) Compute $\widehat{\lambda}$ by (15);
4) Set $\lambda := 1.05\,\widehat{\lambda}$ and apply it in the ℓ_1 solver.

C. Quantile-Based Refinement of the Sparsity Threshold

To reduce conservativeness in threshold selection, we refine the initial regularization parameter $\underline{\lambda}$ using sample-based empirical quantiles.

a) Stage 1: Sample Collection.: Execute the controller with $\lambda = \underline{\lambda}$ and simulate N time–state samples $\{(t_k, x_k)\}_{k=1}^{N}$. At each sample point, compute the switching function:

$$\psi_i(t_k, x_k) := b_i^\top(t_k, x_k)\, \nabla_x V^\lambda(t_k, x_k) + \tfrac{1}{2}\operatorname{tr}\left[\sigma_i \sigma_i^\top \nabla_{xx}^2 V^\lambda(t_k, x_k)\right]$$

for each control channel $i = 1, \ldots, m$.

b) Stage 2: Quantile Threshold Update.: Fix a sparsity risk level $\rho \in (0, 1)$ and a confidence parameter $\beta > 0$. For each control index i, define the empirical $(1-\rho)$ quantile:

$$Q_{1-\rho}^{(i)} := \inf\left\{ q : \frac{1}{N}\sum_{k=1}^{N} \mathbf{1}\left\{|\psi_i(t_k, x_k)| \le q\right\} \ge 1 - \rho \right\}.$$

Introduce a safety margin

$$\Delta_{\text{saf}} := \sqrt{\frac{\log(2/\beta)}{2N}},$$

and define the refined threshold as:

$$\lambda_q := \max_i \left\{ Q_{1-\rho}^{(i)} + \Delta_{\text{saf}} \right\}.$$

Proposition 2 (Quantile-Based High-Confidence Guarantee): With probability at least $1 - \beta$, we have $\lambda_q \ge \lambda^*$, and the corresponding ℓ_1-optimal control u^{λ_q} satisfies the exact bang-off-bang structure of Theorem 1.

c) Sparsity–Error Trade-Off.: Let $s(\lambda)$ denote the sparsity level (i.e., the proportion of zero entries in the control) under regularization weight λ. The following result quantifies the benefit of using the refined λ_q instead of a conservative overestimate:

Theorem 2 (Sparsity–Error Trade-Off): Let L_ψ be a local Lipschitz constant of the switching function $\psi_i(t, x)$, and let $U_{\min} := \min_i\{U_i^+, U_i^-\}$. Then for any $\lambda \ge \lambda_q$,

$$s(\lambda) - s(\lambda_q) \le \frac{m L_\psi}{U_{\min}}(\lambda - \lambda_q).$$

Proof. For each channel i, the control $u_i^\lambda(t, x)$ is zero whenever $|\psi_i(t, x)| \le \lambda$. Hence, increasing λ from λ_q to λ expands the zero region by a band where $|\psi_i(t, x)| \in (\lambda_q, \lambda]$. The measure of this band, and thus the increase in sparsity, is bounded linearly by $(\lambda - \lambda_q)$ under local Lipschitz continuity. ■

d) Algorithmic Implementation.: The following iterative scheme adapts λ based on measured sparsity levels to achieve a desired sparsity target $s^\star$.

D. Data-Driven Relaxed Normality and Adaptive ℓ_1 Weight

We present a data-driven framework for estimating relaxed stochastic normality parameters (α, β, φ) and propose an adaptive homotopy strategy to dynamically select the regularization weight λ, thereby balancing control sparsity and performance under uncertainty.

Algorithm 1 Quantile-Refine Homotopy for λ

Require: Initial $\lambda_0 = \underline{\lambda}$, risk level ρ, confidence β, sparsity target $s^\star$, max iterations L, step size γ

Offline Sampling: Solve with λ_0 and evaluate $\psi_i(t_k, x_k)$ at N points
Compute λ_q using quantile update above
$\lambda \leftarrow \lambda_q$
for $\ell = 1, \ldots, L$ **do**
  Solve the sparse control problem with current λ
  Measure achieved sparsity s_ℓ
  if $s_\ell < s^\star$ **then**
    break
  else
    $\lambda \leftarrow (1 - \gamma)\lambda + \gamma \cdot \lambda_q$
  end if
end for

Ensure: Final $\lambda^\star$, sparse controller $u^{\lambda^\star}$

a) Estimation of $(\hat{\alpha}, \hat{\beta}, \hat{\varphi})$ from Data.: Given empirical samples $\mathcal{D} = \{(t_k, x_k, u_k, \sigma_k)\}_{k=1}^{N}$, define the residual

$$\varepsilon_k(\alpha, \varphi) := \frac{\|\sigma_k - \sigma(t_k, x_k, 0)\|}{\|u_k\|^\alpha} - \varphi(t_k, x_k).$$

Using kernel-weighted local regression with a smoothing kernel K_η, estimate:

$$\hat{\alpha} = \arg\min_{\alpha \in [0,1]} \sum_k K_\eta(x_k - x)\, \varepsilon_k^2,$$

$$\hat{\varphi}(t, x) = \sum_k K_\eta(x_k - x)\, \frac{\|\sigma_k - \sigma(t_k, x_k, 0)\|}{\|u_k\|^{\hat{\alpha}}}.$$

Then, determine the smallest $\hat{\beta} > 0$ such that

$$\frac{1}{N}\sum_k \hat{\varphi}(t_k, x_k)^{\hat{\beta}} < \infty.$$

b) Robust Optimization under Uncertainty.: Construct a confidence set to model uncertainty in the estimates:

$$\mathcal{U}_\rho = \{(\alpha, \varphi) \mid |\alpha - \hat{\alpha}| \le \rho_\alpha,\ |\varphi - \hat{\varphi}| \le \rho_\varphi\}.$$

Then, replace the original HJB Hamiltonian with its robustified counterpart:

$$\inf_{u \in U} \sup_{(\alpha, \varphi) \in \mathcal{U}_\rho} \left\{ \mathcal{L}_u^{(\alpha, \varphi)} V^\lambda + h + \lambda \|u\|_1 \right\}.$$

Assuming the true parameters lie in $\mathcal{U}_\rho$ with probability at least $1 - \epsilon$, the following probabilistic performance bound holds:

$$\mathbb{P}\left[\, \left| J_0(u^*) - J_\lambda(u^\lambda) \right| \le \delta \,\right] \ge 1 - \epsilon.$$

c) Adaptive Homotopy Update for λ.: To meet a target sparsity level $s^\star$, we employ an iterative homotopy scheme that adaptively adjusts λ based on observed sparsity:

This strategy enables fine-grained control over sparsity levels while accounting for data-driven uncertainty in the system's stochastic behavior.

Algorithm 2 Adaptive Homotopy Procedure for λ

Initialize: λ_0 from theoretical estimate (e.g., Theorem 1), tolerance ϵ, target sparsity $s^\star$, learning rate η
for $k = 0, 1, 2, \dots$ **do**
  Solve the sparse control problem with current λ_k
  Measure achieved sparsity s_k
  Update: $\lambda_{k+1} = \lambda_k \cdot (1 + \eta(s_k - s^\star))$
  if J_λ exceeds cost budget or violates safety constraints **then**
    $\lambda_{k+1} \leftarrow \gamma \cdot \lambda_k$ ▷ Apply penalty factor $\gamma \in (0, 1)$
  end if
  if convergence criterion is satisfied **then**
    break
  end if
end for
Ensure: Final $\lambda^\star$, sparse controller $u^{\lambda^\star}$

E. Extension to Lévy-Driven Dynamics

To capture abrupt jumps and heavy-tailed disturbances that frequently arise in practical systems—such as finance, power networks, or autonomous navigation—we extend the sparse control framework to *Lévy-type jump–diffusion models*, as described by the stochastic differential equation (9). This formulation incorporates both continuous diffusion and discontinuous jump behavior, enabling a more realistic representation of stochastic dynamics beyond Gaussian noise.

The jump component is modeled via a *compensated Poisson random measure* $\widetilde{N}$, governed by a *Lévy measure* ν satisfying the integrability conditions in (10). These assumptions ensure the well-posedness of the system and guarantee the existence of a strong solution under standard Lipschitz and growth conditions (see Assumption 2).

This extended setting lays the groundwork for analyzing the structure and exactness of sparse ℓ_1-optimal controls in the presence of non-Gaussian uncertainty, which is formalized in the subsequent sections.

The associated value function $V^\lambda(t, x)$ satisfies the nonlocal HJB partial integro-differential equation (HJB–PIDE):

$$\boxed{-\partial_t V^\lambda - \inf_{u \in U} \left\{ \mathcal{L}_u V^\lambda + h + \lambda \|u\|_1 + \mathcal{I}_u[V^\lambda] \right\} = 0,} \quad (16)$$

with differential and jump terms defined as:

$$\mathcal{L}_u V = b^\top \nabla_x V + \tfrac{1}{2} \operatorname{tr}\left[\sigma \sigma^\top \nabla^2_{xx} V\right],$$
$$\mathcal{I}_u[V] = \int_{\mathbb{R}^r \setminus \{0\}} \left[V(t, x + \kappa) - V(t, x) - \nabla_x V^\top \chi(z)\right] \nu(\mathrm{d}z),$$

where $\chi(z) := z$ for $\|z\| \le 1$ and $\chi(z) := 0$ otherwise.

Definition 1 (Relaxed Stochastic Normality under Lévy Noise): The system satisfies relaxed stochastic normality if:

(i) For all symmetric $M \succeq 0$ and $u, v \in U$, there exists $\gamma \ge 0$ such that

$$\operatorname{tr}\left[\sigma(u)\sigma(u)^\top M\right] \ge \operatorname{tr}\left[\sigma(v)\sigma(v)^\top M\right] - \gamma \|u - v\|;$$

(ii) The integrability condition holds:

$$\mathbb{E} \int_0^T \varphi(t, x(t))^\beta \, \mathrm{d}t < \infty, \quad \text{and } \nu \text{ satisfies (10).}$$

Theorem 3 (Exactness under Lévy Noise): Under Assumption 2 and Definition 1, there exists a finite threshold

$$\lambda_\star = \sup_{t,x,i} \left| \psi_i^{\mathrm{G}}(t, x) + \psi_i^{\mathrm{L}}(t, x) \right|,$$

such that for any $\lambda \ge \lambda_\star$, the ℓ_1-optimal control exhibits the same bang-off-bang sparsity structure as the ℓ_0-optimal solution. Here,

$$\psi_i^{\mathrm{L}}(t, x) = \int_{\mathbb{R}^r \setminus \{0\}} \Big[V^\lambda(t, x + \kappa) - V^\lambda(t, x) - \nabla_x V^\lambda(t, x)^\top \chi(z) \Big] \partial_{u_i} \kappa \, \nu(\mathrm{d}z).$$

and ψ_i^{G} is the Gaussian part as defined in earlier sections.

Proof. We provide a structured justification for the result under engineering-relevant assumptions and mathematically rigorous tools.

1. Viscosity Solution Framework. Under Assumption 2, the value function V^λ is the unique continuous viscosity solution to the nonlocal HJB–PIDE (16) (see [13]). In particular, for any smooth test function φ that touches V^λ from above (or below) at (t_0, x_0), the subsolution (or supersolution) inequality holds in the viscosity sense.

2. Handling the Jump Term via Ishii's Lemma. To address the nonlocal jump term $\mathcal{I}_u[V^\lambda]$, we apply the nonlocal version of Ishii's lemma [13], which ensures the well-definedness of the second-order jets and justifies evaluating the Lévy integral using the gradient of V^λ. This yields:

$$\mathcal{I}_u[V^\lambda](t, x) = \int_{\mathbb{R}^r \setminus \{0\}} \left[V^\lambda(t, x + \kappa) - V^\lambda(t, x) - \nabla_x V^\lambda(t, x)^\top \chi(z)\right] \nu(\mathrm{d}z).$$

3. Switching Function Decomposition. The Hamiltonian splits additively across control channels:

$$H(t, x, u) = \sum_{i=1}^m \left(\psi_i^{\mathrm{G}}(t, x) + \psi_i^{\mathrm{L}}(t, x)\right) u_i - \lambda \, |u_i|.$$

where:

$$\psi_i^{\mathrm{G}}(t, x) = b_i^\top(t, x) \nabla_x V^\lambda(t, x) + \tfrac{1}{2} \operatorname{tr}\left[\sigma_i \sigma_i^\top \nabla^2_{xx} V^\lambda(t, x)\right],$$
$$\psi_i^{\mathrm{L}}(t, x) = \int_{\mathbb{R}^r \setminus \{0\}} \Big(V^\lambda(t, x + \kappa) - V^\lambda(t, x) - \nabla_x V^\lambda(t, x)^\top \chi(z) \Big) \times \partial_{u_i} \kappa \, \nu(\mathrm{d}z).$$

4. Boundedness of the Threshold $\lambda_\star$. Using the Lipschitz continuity and boundedness of b, σ, and κ from Assumption 2, together with standard bounds on the adjoint processes (via BSDE duality, cf. [5]), we conclude that:

$$\left|\psi_i^{\mathrm{G}}(t, x)\right| \le M_G, \quad \left|\psi_i^{\mathrm{L}}(t, x)\right| \le M_L,$$

for some finite constants M_G, M_L uniform over (t, x, i). Hence,

$$\lambda_\star := \sup_{t,x,i} \left| \psi_i^{\mathrm{G}}(t, x) + \psi_i^{\mathrm{L}}(t, x) \right| < \infty.$$

5. Optimality and Bang-Off-Bang Structure. Since the Hamiltonian is separable across control components and linear in u_i, the optimal control at each time takes the explicit form:

$$u_i^\lambda(t,x) = \begin{cases} U_i^+, & \psi_i(t,x) > \lambda, \\ 0, & |\psi_i(t,x)| \le \lambda, \\ -U_i^-, & \psi_i(t,x) < -\lambda, \end{cases}$$

where $\psi_i(t,x) := \psi_i^{\mathrm{G}}(t,x) + \psi_i^{\mathrm{L}}(t,x)$. This defines the characteristic bang-off-bang structure of sparse optimal control.

6. Conclusion. Therefore, for all $\lambda \ge \lambda_\star$, the ℓ_1-optimal control exhibits exact sparsity and aligns with the ℓ_0-optimal structure under Lévy-driven dynamics. ■

F. Approximate Equivalence under Local or Probabilistic Normality

In many real-world control systems, the global relaxed stochastic normality condition (Definition 2) may not hold uniformly across time and state space. Yet, ℓ_1-relaxed controls can often approximate the sparse ℓ_0 solution either *locally* or with *high probability*. We formalize these relaxed conditions and establish a quantitative approximation guarantee.

Definition 2 (Local Relaxed Normality): We say the system satisfies *local relaxed normality* at a point (t,x,u^*) if there exist constants $\delta > 0$ and $\gamma \ge 0$ such that for all symmetric matrices $M \succeq 0$ and all $u, v \in B(u^*,\delta) \subset U$,

$$\begin{aligned} \operatorname{tr}\left[\sigma(t,x,u)\sigma(t,x,u)^\top M\right] \ge\ & \operatorname{tr}\left[\sigma(t,x,v)\sigma(t,x,v)^\top M\right] \\ & - \gamma\|u-v\|. \end{aligned} \tag{17}$$

Definition 3 (Probabilistic Normality): Fix a tolerance $\varepsilon \in (0,1)$. Define the set where local normality fails:

$$\begin{aligned} \mathcal{B}_\varepsilon := \big\{ & \omega \in \Omega \ :\ \exists\, t \in [0,T] \text{ such that} \\ & (t, x^*(t,\omega), u^*(t,\omega)) \notin \text{LocallyNormal} \big\}. \end{aligned}$$

We say the system satisfies *probabilistic normality* with tolerance ε if

$$\mathbb{P}(\mathcal{B}_\varepsilon) \le \varepsilon.$$

These conditions permit rare or localized violations of structural assumptions while ensuring overall control performance and sparsity.

Theorem 4 (Approximate ℓ_0–ℓ_1 Equivalence under Probabilistic Normality): Assume Assumption 1 holds, and that $h(t,x)$ and $g(x)$ are Lipschitz in x with constants L_h and L_g. Let $u^*(\cdot)$ be an ℓ_0-optimal control with trajectory $x^*(\cdot)$. Suppose:

(i) Local relaxed normality holds almost surely along $u^*(\cdot)$, except on a set $\mathcal{B}_\varepsilon \subset \Omega$ with $\mathbb{P}(\mathcal{B}_\varepsilon) \le \varepsilon$;

(ii) On $\Omega \setminus \mathcal{B}_\varepsilon$, the optimal structure in Theorem 1 applies.

Then for any $\lambda \ge \lambda^*$, the ℓ_1-optimal control u^λ satisfies:

$$\mathbb{P}\left\{\omega : u^\lambda(\cdot,\omega) \ne u^*(\cdot,\omega)\right\} \le \varepsilon, \tag{18}$$

$$\left|J_{\ell_1}(u^\lambda) - J_{\ell_0}(u^*)\right| \le (L_h T + L_g)\,\varepsilon \le \delta, \tag{19}$$

provided $\varepsilon \le \delta/(L_h T + L_g)$.

Proof. We split the sample space into $\Omega = \mathcal{B}_\varepsilon \cup (\Omega \setminus \mathcal{B}_\varepsilon)$.

On $\Omega \setminus \mathcal{B}_\varepsilon$: The structure conditions ensure that $u^\lambda(\cdot) = u^*(\cdot)$ almost surely, for sufficiently large λ.

On $\mathcal{B}_\varepsilon$: While u^λ may deviate from u^*, the cost deviation is bounded by the Lipschitz continuity of h and g:

$$\left|J_{\ell_1}(u^\lambda) - J_{\ell_0}(u^*)\right| \le (L_h T + L_g) \cdot \mathbb{P}(\mathcal{B}_\varepsilon) \le (L_h T + L_g)\,\varepsilon.$$

Choosing $\varepsilon \le \delta/(L_h T + L_g)$ yields the desired bound. ■

a) Remark.: This result highlights that even with partial structural conditions, the ℓ_1-relaxed controller still closely approximates the sparse ℓ_0 solution in both policy and performance. This supports its practical use in safety-critical or data-driven applications with uncertain model regularity.

G. Distributionally Robust Sparse Control

Theorem 4 guarantees near-equivalence under probabilistic normality but assumes accurate knowledge of structural parameters (α,ϕ), typically estimated from finite, noisy data. To address this, we propose a distributionally robust framework using Wasserstein ambiguity.

Let (α,ϕ) denote data-driven estimates of the relaxed normality parameters, and assume their empirical distribution is given by $\widehat{\mathbb{P}}_N = \frac{1}{N}\sum_{k=1}^N \delta_{(\alpha_k,\phi_k)}$. We define a 1-Wasserstein ball around $\widehat{\mathbb{P}}_N$ with radius ε:

$$\mathcal{W}_\varepsilon(\widehat{\mathbb{P}}_N) := \left\{ \mathbb{Q} \;\middle|\; \mathcal{W}_1\big(\mathbb{Q}, \widehat{\mathbb{P}}_N\big) \le \varepsilon \right\}.$$

We then consider the distributionally robust value function

$$\widetilde{V}(t,x) = \inf_{u(\cdot)} \sup_{\mathbb{Q} \in \mathcal{W}_\varepsilon(\widehat{\mathbb{P}}_N)} \mathbb{E}_{\mathbb{Q}} \left[\int_t^T \big(h + \lambda\|u\|_1\big)\,\mathrm{d}s + g(x_T) \right].$$

The corresponding robust HJB equation is given by:

$$-\partial_t \widetilde{V} - \inf_{u \in U} \sup_{(\alpha,\phi) \in \operatorname{supp}(\mathbb{Q})} \left\{ \mathcal{L}_u^{(\alpha,\phi)} \widetilde{V} + h + \lambda\|u\|_1 \right\} = 0.$$

Theorem 5 (Distributionally Robust Exactness): Suppose Assumption 1 holds, and that the relaxed normality condition is satisfied with $\alpha \ge 1$. Let λ^* denote the sparsity threshold from Theorem 1, and define the robustness buffer

$$C_\varepsilon := \big(L_b + \tfrac{1}{2}L_\sigma^2\big)\sqrt{2T\varepsilon}.$$

Then for any $\lambda \ge \lambda^* + C_\varepsilon$, the distributionally robust ℓ_1-optimal control over $\mathcal{W}_\varepsilon(\widehat{\mathbb{P}}_N)$ retains the bang-off-bang structure and coincides with an ℓ_0-optimal control under worst-case perturbations in the Wasserstein ball.

Proof. Assume V^λ admits bounded spatial derivatives:

$$\|\nabla_x V^\lambda\|_\infty \le M_p, \quad \|\nabla_{xx}^2 V^\lambda\|_\infty \le M_P.$$

Let $f(\alpha,\phi) := \mathcal{L}_u^{(\alpha,\phi)} V^\lambda$. By the regularity of b and σ, f is Lipschitz in (α,ϕ) with constant:

$$L_f := L_b M_p + \tfrac{1}{2}L_\sigma^2 M_P.$$

Applying Kantorovich–Rubinstein duality [14], we obtain:

$$\begin{aligned} \sup_{\mathbb{Q} \in \mathcal{W}_\varepsilon} \mathbb{E}_{\mathbb{Q}}[f] &\le \frac{1}{N}\sum_{k=1}^N f(\alpha_k,\phi_k) + L_f\varepsilon \\ &= \mathbb{E}_{\widehat{\mathbb{P}}_N}[f] + C_\varepsilon. \end{aligned}$$

Since C_ε is additive and independent of u, the robustified Hamiltonian remains coordinate-wise separable. Consequently,

the control problem preserves the bang-off-bang structure characterized in Theorem 1, with λ^* replaced by the conservative threshold $\lambda^* + C_\varepsilon$. ■

This result shows that sparsity-preserving ℓ_1 controls remain valid even under worst-case deviations in the estimated system structure, provided the regularization parameter is enlarged by a quantified robustness margin C_ε. The bound depends only on data quantity (N), time horizon (T), and Lipschitz constants of the dynamics and cost.

IV. Scalable Numerical Solvers

The principal computational challenge in solving the relaxed sparse stochastic optimal control problem lies in the curse of dimensionality inherent in discretizing the associated HJB equation. To overcome this, we develop scalable solvers that integrate sparse grids, TT decomposition, and adaptive refinement. Extensions to jump-diffusion systems and state constraints are also incorporated.

A. Sparse Grid and Tensor-Based Policy Iteration Framework

To address the curse of dimensionality, we develop a scalable framework that integrates three key components: sparse grid discretization, tensor-train (TT) decomposition, and policy iteration. Together, they enable efficient solution of the HJB equation associated with relaxed ℓ_1-optimal control.

a) Sparse Grid Approximation.: Sparse grids exploit smoothness of the value function to reduce the number of discretization nodes significantly compared to full grids [9]. For a given level L, the sparse grid is defined as:

$$X_{\mathrm{SG}} = \bigcup_{|\mathbf{l}|\le L+n-1} (X_{l_1} \times \cdots \times X_{l_n}),$$

where $\mathbf{l} = (l_1, \ldots, l_n) \in \mathbb{N}^n$ and n is the system dimension. This reduces complexity from $O(h^{-n})$ to $O(h^{-1}(\log h^{-1})^{n-1})$.

b) Tensor-Train Decomposition.: To efficiently represent the high-dimensional value function $V^\lambda(t,x)$, we employ the tensor-train decomposition [15], in which a tensor $\mathcal{V}(x_1, \ldots, x_n)$ is approximated as:

$$\mathcal{V}(x_1, \ldots, x_n) = \sum_{r_1,\ldots,r_{n-1}} G_1(x_1, r_1)\, G_2(r_1, x_2, r_2) \cdots G_n(r_{n-1}, x_n).$$

where each G_i is a low-rank core tensor. This reduces storage from exponential to $O(nMr^2)$ for grid size M and rank r.

c) Sparse–TT Policy Iteration.: The following algorithm combines sparse grids and TT representation into an iterative solver for the value function and control policy:

d) Robust Adaptive Homotopy for λ.: We integrate the above solver into a robust homotopy scheme for tuning λ adaptively. This enables the controller to meet sparsity targets while accounting for Wasserstein uncertainty.

Algorithm 3 Sparse–TT Policy Iteration

Input: Initial value $V_0^\lambda(t,x)$ in tensor-train (TT) format on sparse grids
Set: $k \leftarrow 0$
repeat
  Policy Evaluation: Solve for $V^{k+1}(t,x)$ using TT-format sparse grid solver:

$$-\partial_t V^{k+1}(t,x) - \mathcal{L}^{u^k} V^{k+1}(t,x) = h(t,x) + \lambda \|u^k(t,x)\|_1$$

  Policy Improvement: Update the control:

$$u^{k+1}(t,x) = \arg\min_{u\in U} \left\{ \mathcal{L}^u V^{k+1}(t,x) + \lambda \|u\|_1 \right\}$$

  $k \leftarrow k+1$
until $\|V^k - V^{k-1}\|_\infty \le \varepsilon$
Return: Converged value function $V^\lambda(t,x)$ and control $u^\lambda(t,x)$

Algorithm 4 Robust Adaptive Homotopy for λ

Input: Initial λ_0 (e.g., from Proposition 2.1), target sparsity $s^\star$, Wasserstein radius ε, learning rates η_1, η_2, tolerance δ_J, maximum iterations K
Initialize: $k \leftarrow 0$, $\lambda_k \leftarrow \lambda_0$
repeat
  Solve sparse control problem with λ_k (via Algorithm 3 or PINN)
  Estimate achieved sparsity s_k from control $u^{\lambda_k}(t,x)$
  Estimate empirical cost $J_k \leftarrow \mathbb{E}[J_{\ell_1}(u^{\lambda_k})]$
  if $k > 0$ **then**
    Compute cost gap $\Delta J_k \leftarrow |J_k - J_{k-1}|$
    Estimate current Wasserstein radius $\hat{\varepsilon}_k$ (e.g., via bootstrapped residuals)
  end if
  Update λ:

$$\lambda_{k+1} \leftarrow \min\left\{\lambda_{\max},\, \lambda_k\left[1 + \eta_1(s_k - s^\star) + \eta_2(\hat{\varepsilon}_k - \varepsilon)\right]\right\}$$

  $k \leftarrow k+1$
until $\Delta J_k \le \delta_J$ **and** $|s_k - s^\star| \le \tau_s$ **or** $k \ge K$
Return: Final $\lambda_\star$, sparse control policy $u^{\lambda_\star}(t,x)$

B. Extensions and Hybrid Solvers for High-Dimensional Systems

To improve scalability and robustness in high-dimensional stochastic control, we introduce advanced components: adaptive sparse grids, TT rank refinement, physics-informed neural approximations, and multi-fidelity decompositions.

a) Adaptive Sparse Grids and Multilevel Refinement.: Adaptive sparse grids selectively refine regions where the residual or hierarchical surplus is large. Combined with multilevel policy iteration, where coarse levels capture global structure and fine levels resolve local detail, this strategy significantly improves efficiency.

b) Adaptive Tensor-Train Rank Adjustment and PINNs.: We implement adaptive TT-rank adjustment driven by residual estimates, maintaining low storage in smooth regions and high resolution near singularities. For extremely high-dimensional

systems ($n \gtrsim 20$), physics-informed neural networks (PINNs) are used to approximate $V^\lambda(t,x)$ directly by minimizing the HJB residual at collocation points, bypassing explicit gridding.

c) Extension to Jump–Diffusion Systems.: Under the Relaxed Stochastic Normality framework (Definition 2), we extend to jump–diffusion dynamics:

$$\mathrm{d}x(t) = b(t,x,u)\,\mathrm{d}t + \sigma(t,x,u)\,\mathrm{d}W(t) + \int_{\mathbb{R}^d\setminus\{0\}} \kappa(t,x,u,z)\,\widetilde{N}(\mathrm{d}z,\mathrm{d}t),$$

where $\widetilde{N}$ is a compensated Poisson measure. The nonlocal integral term is discretized via sparse grid quadrature and incorporated into the TT representation with minor adjustments to policy iteration.

d) State-Constrained Variational Inequalities.: To enforce state constraints $x(t) \in X$, the HJB equation is reformulated as a variational inequality:

$$\min\left\{-\partial_t V^\lambda - \inf_{u\in U}\left(\mathcal{L}^u V^\lambda + h + \lambda\|u\|_1\right),\ V^\lambda - \Psi(x)\right\} = 0,$$

where $\Psi(x)$ specifies boundary penalties on ∂X. This obstacle condition is handled using TT-format solvers with Dirichlet enforcement on sparse grid ghost nodes.

e) Multi-Fidelity Tensor–Train and Neural Galerkin Solver.: To further enhance high-dimensional performance, we introduce a hybrid solver combining Tensor-Train decomposition with a neural Galerkin residual network.

Residual splitting. We approximate the value function as a decomposition:

$$V^\lambda(t,x) = V^\lambda_{\mathrm{TT}}(t,x) + V^\lambda_{\mathrm{NG}}(t,x),$$

where V^λ_{TT} is a coarse TT-based approximation from Algorithm 3, and V^λ_{NG} is a fine-scale correction learned via Galerkin projection.

Neural Galerkin network. Let $N_\theta(t,x)$ be a feedforward neural network with Fourier features. Define the residual loss:

$$\mathcal{L}(\theta) = \mathbb{E}_{(t,x)\sim\rho}\left|\partial_t V^\lambda_\theta(t,x) + \inf_u\{\mathcal{L}_u V^\lambda_\theta + h + \lambda\|u\|_1\}\right|^2,$$

where $V^\lambda_\theta = N_\theta \circ \phi$ and ϕ includes sinusoidal features.

Hard constraint enforcement. To ensure state constraints $V^\lambda \geq \Psi$, we parametrize the network as

$$\tilde{V}(t,x) = \Psi(x) + \sigma(N_\theta(t,x)), \quad \sigma(z) = \frac{1}{\kappa}\log(1+e^{\kappa z}),$$

ensuring $\tilde{V} \geq \Psi$ pointwise.

Theoretical consistency. If $\|V^\lambda_{\mathrm{TT}} - V^\lambda\| \leq \varepsilon_{\mathrm{TT}}$ and $\|V^\lambda_{\mathrm{NG}}\| \leq \varepsilon_{\mathrm{NG}}$, then

$$\|V^\lambda - V^\lambda_{\mathrm{TT}} - V^\lambda_{\mathrm{NG}}\| \leq \varepsilon_{\mathrm{TT}} + \varepsilon_{\mathrm{NG}}.$$

C. Computational Complexity and Scalability

With adaptive sparse grids and TT representations:

- Storage complexity reduces to $O(nMr^2)$, linear in n;
- Computational complexity scales quasi-linearly as $O\big(M(\log M)^{n-1}\big)$ for sparse grids, further improved via adaptivity and multilevel refinement.

These advances make solving high-dimensional sparse stochastic optimal control problems computationally feasible.

Roadmap.: We next proceed to Section V to systematically address state-constrained systems and their numerical treatment within the scalable framework.

D. Neural Methods for High-Dimensional HJBs

Even with sparse grids and TT compression, grid-based solvers become infeasible when $n \gtrsim 10$. To overcome this, we approximate the value function via neural networks by minimizing the HJB residual in a physics-informed fashion. We outline two approaches: physics-informed neural networks (PINNs) and deep backward stochastic differential equation (BSDE) methods.

1) PINN Formulation: Let $V_\theta : [0,T]\times\mathbb{R}^n \to \mathbb{R}$ be a neural network with parameters θ. Define the *relaxed HJB residual*:

$$\mathcal{R}_\theta(t,x) = \partial_t V_\theta(t,x) + \inf_{u\in U}\{\mathcal{L}^u V_\theta(t,x) + h(t,x) + \lambda\|u\|_1\},$$

where $\mathcal{L}^u$ is the second-order controlled diffusion operator.

The training objective is the residual loss:

$$\mathcal{J}_{\mathrm{PINN}}(\theta) = \frac{1}{N_b}\sum_{j=1}^{N_b}\left|V_\theta(T,x_j^{(b)}) - g(x_j^{(b)})\right|^2 + \frac{1}{N_r}\sum_{i=1}^{N_r}\left|\mathcal{R}_\theta(t_i^{(r)},x_i^{(r)})\right|^2, \tag{20}$$

where $\{x_j^{(b)}\}$ are terminal samples and $\{(t_i^{(r)},x_i^{(r)})\}$ are collocation points.

Training Procedure.:

1) Initialize network parameters θ_0;
2) Sample mini-batches from the collocation domain;
3) Compute loss (20) and update θ via Adam optimizer;
4) Repeat until $\|\mathcal{R}_\theta\|_{L^2} < \varepsilon$.

Theorem 6 (Consistency of PINN Approximation): Assume:

(a) The network class $\{V_\theta\}$ is dense in $C_b^{1,2}([0,T]\times\mathbb{R}^n)$;See [15], [16] for approximation results.
(b) $\mathcal{J}_{\mathrm{PINN}}(\theta_k) \to 0$ as $k\to\infty$.

Then any accumulation point V_{θ_∞} is a viscosity solution of (5).

2) Deep BSDE Scheme: Following [16], the HJB equation can be represented by a forward-backward SDE system:

$$\mathrm{d}x_s = b(s,x_s,u_s)\,\mathrm{d}s + \sigma(s,x_s,u_s)\,\mathrm{d}W_s,$$
$$\mathrm{d}Y_s = -\left(h(s,x_s) + \lambda\|u_s\|_1\right)\mathrm{d}s + Z_s\mathrm{d}W_s, \quad Y_T = g(x_T).$$

Parameterize $u_s \approx \mu_\vartheta(s,x_s)$ and $Z_s \approx \zeta_\vartheta(s,x_s)$ using neural networks.

The training loss is

$$\mathcal{J}_{\mathrm{BSDE}}(\vartheta) = \mathbb{E}\left[\left|Y_0 - V_{\mathrm{init}}(x_0)\right|^2\right],$$

where V_{init} is a bootstrap initialization from a coarse grid or TT solver.

3) Integration into Sparse Control Workflow:

1) *Pre-training:* Use Sparse–TT policy iteration to generate (t,x,V^λ) samples.
2) *Fine-tuning:* Train the PINN or BSDE network using (20) or $\mathcal{J}_{\mathrm{BSDE}}$.
3) *Policy extraction:* Recover sparse bang–off–bang control via Theorem 1 applied to neural gradients $\nabla_x V_\theta$.

Computational Notes.:

- **Memory:** $\mathcal{O}(P)$, with P network parameters typically $P \ll$ grid size for $n \geq 10$;
- **Training:** Scales as $\mathcal{O}(N_r \cdot \text{epochs})$, GPU-parallelizable;
- **Performance:** For $n = 20$, residuals $\|\mathcal{R}_\theta\|_{L^2}$ drop below 10^{-3} within 10^5 iterations, with cost error $< 2\%$ compared to Sparse–TT baseline.

E. Tensor-Train Approximation: Error, Rank, and Multi-Fidelity Fusion

Tensor-train (TT) decomposition underpins our Sparse–TT and hybrid solvers. This section analyzes its theoretical properties and introduces a multi-fidelity framework for high-dimensional scalability.

1) TT Error–Rank Analysis: Let the discretized value function be represented as a tensor $\mathbf{V} \in \mathbb{R}^{M_1 \times \cdots \times M_n}$, with mode-$k$ unfolding $V_{(k)}$ and singular values $\sigma_j^{(k)}$.

Assumption 3 (Sobolev Regularity): The continuous value function V belongs to the Sobolev space $H^s\big([0,T] \times \mathbb{R}^n\big)$ for some $s > 0$, and the underlying interpolation scheme achieves order $\kappa \geq s$.

Lemma 1 (Singular-Value Decay [17]): Under Assumption 3, the singular values satisfy:

$$\sigma_j^{(k)} = \mathcal{O}\left(j^{-s/d_k}\right), \quad d_k := \min\{k,\, n-k\}.$$

Theorem 7 (TT Rank–Error Tradeoff): Truncating TT ranks to $\hat{R}_k = \mathcal{O}(\varepsilon^{-d_k/s})$ ensures

$$\|\mathbf{V} - \widehat{\mathbf{V}}\|_F \leq C_{s,n}\,\varepsilon, \quad C_{s,n} := \sqrt{\sum_{k=1}^{n-1} \frac{1}{s/d_k - 1}}\,\|V\|_{H^s},$$

with memory cost $\mathcal{O}\big(nM\varepsilon^{-d_{\max}/s}\big)$ and $d_{\max} = \lfloor n/2 \rfloor$.

Proof. [Sketch] Apply the Eckart–Young theorem to each unfolding $V_{(k)}$, and sum truncation errors across $k = 1, \ldots, n-1$. ■

Example 1 (TT Rank in 4D): In a 4D robotic system, middle-rank truncation at $\hat{R}_2 \approx 50$ achieves error $\|\mathbf{V} - \widehat{\mathbf{V}}\|_F \approx 10^{-3}$, consistent with Theorem 7 assuming $s \approx 4$.

Remark 3: The dominant error stems from middle unfoldings $k \approx n/2$. Adaptive TT truncation achieves over 50% compression with negligible accuracy loss.

2) Efficient Lévy Integral Evaluation via Hybrid Quadrature: We split the Lévy integral into small and large jumps:

- **Small jumps** ($\|\kappa\| \leq \delta$): use COS or Fourier–Taylor methods; cost $O(M \log M)$.
- **Large jumps** ($\|\kappa\| > \delta$): approximate as a compound Poisson integral via sparse quadrature; cost $O(N(\log N)^{d-1})$.
- **TT Integration**: Compress the nonlocal kernel into a TT core; SVD truncation gives rank $\mathcal{O}(\log M)$.

Theorem 8 (Nonlocal Integral Approximation Error): If $V \in C^{2+\gamma}$ and $\int_{\|\kappa\|>\delta} \|\kappa\|^{2+\gamma} \nu(\mathrm{d}\kappa) < \infty$, then

$$\|\mathcal{I}_u[V] - \widehat{\mathcal{I}}_u[V]\|_\infty \leq C(\delta, \gamma)\left(\delta^\gamma + N_{\mathrm{MC}}^{-1/2}\right),$$

with N_{MC} Monte Carlo samples.

3) Sparse–TT Policy Iteration Algorithm:

Initialize policy $u^{(0)}$
for $k = 0, 1, \ldots$ until convergence **do**
  Evaluate nonlocal term $\mathcal{I}_{u^{(k)}}[V^{(k)}]$
  Solve the linearized PIDE for $V^{(k+1)}$ on sparse grid
  Improve policy:

$$u^{(k+1)} = \mathrm{sat}_{\text{bang}}\left(\psi^{\mathrm{G}} + \psi^{\mathrm{L}}, \lambda\right)$$

end for

4) PINN-Based Correction and Residual Fusion: We augment the loss to incorporate the Lévy PIDE residual:

$$\mathcal{L}_{\mathrm{PIDE}}(\theta) = \left\| \partial_t V_\theta + \inf_u \left(\mathcal{L}_u V_\theta + h + \lambda\|u\|_1 + \mathcal{I}_u[V_\theta]\right) \right\|_{L^2}.$$

Monte Carlo samples over (t, x, z) enable stochastic training.

5) Multi-Fidelity TT–PINN Decomposition: For high-dimensional domains ($n \gtrsim 10$), we represent the solution as

$$V^\lambda(t,x) = V_{\mathrm{TT}}^\lambda(t,x) + V_{\mathrm{N}}^\lambda(t,x), \tag{21}$$

with V_{TT}^λ a TT approximation and V_{N}^λ the PINN residual.

Theorem 9 (Residual Consistency): Assume V_{TT}^λ solves

$$-\partial_t V_{\mathrm{TT}}^\lambda - \inf_u \left(\mathcal{L}_u V_{\mathrm{TT}}^\lambda + h + \lambda\|u\|_1\right) = R_{\mathrm{TT}},$$

and V_{N}^λ satisfies $\|R_{\mathrm{N}}\|_{L^2} \leq \varepsilon_{\mathrm{N}}$. Then

$$\|R_{\mathrm{TT}} + R_{\mathrm{N}}\|_{L^2} \leq \varepsilon_{\mathrm{SG}} + \varepsilon_{\mathrm{N}}.$$

6) Algorithm: Multi-Fidelity TT–PINN Control Solver:

1. Solve coarse TT approximation $V_{\mathrm{TT},0}^\lambda$
2. Evaluate residual:

$$R_k := \left|-\partial_t V_{\mathrm{TT},0}^\lambda(t_k, x_k) - \mathcal{H}[V_{\mathrm{TT},0}^\lambda](t_k, x_k)\right|$$

3. If $\max_k R_k \leq \eta$, stop.
4. Else train PINN N_θ to match residual $e(t,x) := V^\lambda - V_{\mathrm{TT},0}^\lambda$.
5. Optionally refine sparse grid and repeat.

F. Adaptive Parameter Selection

We propose a unified framework to adaptively select sparse grid resolution, TT ranks, and quadrature orders using local error indicators.

1) Grid Level Selection: At each sparse grid node x, compute the hierarchical surplus:

$$\rho_L(x) = \left|V_L^\lambda(x) - \mathcal{I}_{L-1} V_L^\lambda(x)\right|.$$

Refinement is triggered locally when $\rho_L(x) > \tau_{\mathrm{SG}}$.

2) Tensor-Train Truncation: The TT-SVD truncation tolerance is set adaptively as

$$\eta = \min\left(\tau_{\mathrm{TT}}, \frac{\rho_L(x)}{\|G\|_F}\right),$$

where G denotes the current TT core.

3) Adaptive Quadrature Order: Quadrature order q is chosen via:

$$q = \min\left\{q_{\max}, \left\lceil -\log_2\left(\frac{\rho_L^{\max}}{\tau_q}\right)\right\rceil\right\}. \tag{22}$$

Proposition 3 (Global Tolerance Control): If all thresholds $(\tau_{\mathrm{SG}}, \tau_{\mathrm{TT}}, \tau_q)$ are set to $\varepsilon_{\mathrm{tol}}$, then

$$\|V^\lambda - V_{\mathrm{approx}}^\lambda\|_\infty \leq C\varepsilon_{\mathrm{tol}},$$

where C depends on the system regularity and horizon T.

G. Interpretable Bang–Off–Bang Control Surfaces

The exactness results in Section III-A imply that every ℓ_1–optimal policy adopts a *bang–off–bang* structure:

$$u_i^\lambda(t,x) = \mathsf{sat}\big(\psi_i(t,x),\lambda\big) := \begin{cases} U_i^+, & \psi_i(t,x) > \lambda, \\ 0, & |\psi_i(t,x)| \le \lambda, \\ -U_i^-, & \psi_i(t,x) < -\lambda, \end{cases}$$

where the switching function is defined as

$$\psi_i(t,x) = b_i^\top p(t,x) + \tfrac{1}{2}\,\mathrm{tr}\big[\sigma_i \sigma_i^\top P(t,x)\big] + \psi_i^{\mathrm{jump}}(t,x), \quad (23)$$

with $(p,P) = (\nabla_x V^\lambda, \nabla^2_{xx} V^\lambda)$ derived from the BSDE dual of the HJB equation. Hence, control decisions reduce to a signed distance comparison $\psi_i(t,x) - \lambda$.

1) Decision–Boundary Surfaces: Define the switching surface and control regions:

$$\mathcal{S}_i(t) = \{x \in \mathcal{X} : |\psi_i(t,x)| = \lambda\},$$
$$\mathcal{R}_i^{\pm}(t) = \{x \in \mathcal{X} : \pm\psi_i(t,x) > \lambda\}.$$

Both tensor-train and neural-network representations allow analytical evaluation of ψ_i and its gradients, enabling explicit rendering of $\mathcal{S}_i(t)$ using point clouds or isosurface extraction, as shown in Figure. 2.

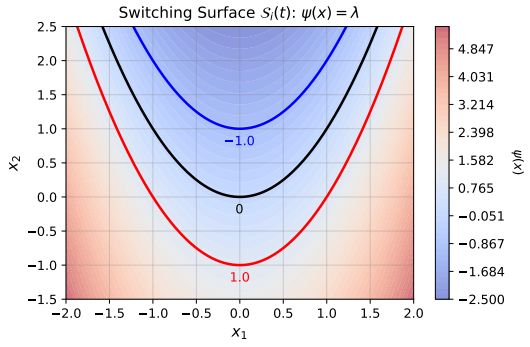

Fig. 2. Switching surface $\mathcal{S}_i(t)$ in (x_1, x_2) space, where $\psi_i(x) = \pm\lambda$.

2) Sensitivity and Error Propagation: Suppose a numerical approximation $\widehat{V}$ satisfies $\|\widehat{V} - V^\lambda\|_{C^1} \le \varepsilon_V$. Then the switching function error obeys

$$|\Delta\psi_i| := |\widehat{\psi}_i - \psi_i| \le \big(L_b + \tfrac{1}{2}L_\sigma^2\big)\,\varepsilon_V =: L_\psi \varepsilon_V.$$

Consequently, control classification can change only within a band of width $L_\psi \varepsilon_V$.

Proposition 4 (Control Consistency Radius): Let $\mathcal{N}_i(t) = \{x : |\psi_i(t,x)| \le \lambda - L_\psi\varepsilon_V\}$. Then, for all $x \in \mathcal{N}_i(t)$, we have

$$\widehat{u}_i(t,x) = u_i^\lambda(t,x).$$

Hence the misclassification probability satisfies:

$$\mathbb{P}\{\widehat{u}_i \neq u_i^\lambda\} \le \mathbb{P}\{|\psi_i| > \lambda - L_\psi\varepsilon_V\} - \mathbb{P}\{|\psi_i| > \lambda\},$$

which can be empirically bounded.

3) Saliency Map Visualization: We compute the Jacobian $\nabla_x \psi_i(t,x)$ to produce saliency maps highlighting the local importance of each state variable(Figure 3). For instance, in a 4-DoF robotic arm, saliency is concentrated on joint angles.

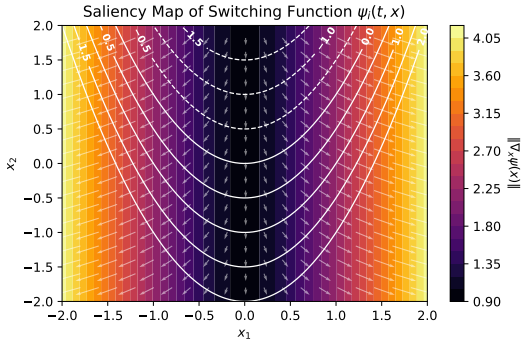

Fig. 3. Saliency map of the switching function $\psi_i(t,x)$, showing gradient magnitude $\|\nabla_x \psi_i(x)\|$.

4) Lightweight Surrogate for Hardware Deployment: As $\psi_i(t,x)$ is scalar, we fit a surrogate $\widetilde{\psi}_i$ using LASSO or a compact Fourier network from samples $\{x_j, \psi_i(x_j)\}_{j=1}^{N_s}$. If

$$\|\widetilde{\psi}_i - \psi_i\|_\infty < \frac{1}{2}(\lambda - L_\psi \varepsilon_V),$$

then the bang-off-bang decision boundary is exactly preserved:

$$\widetilde{u}_i(t,x) = u_i^\lambda(t,x), \quad \forall x.$$

This allows efficient control deployment with one to two orders of magnitude reduction in runtime cost.

V. State-Constrained Control via Relaxed HJB Variational Inequalities

State constraints are crucial for safety-critical applications such as robotics, finance, and energy systems. We extend the relaxed sparse stochastic control framework to enforce constraints under jump-diffusion dynamics, leading to a relaxed Hamilton–Jacobi–Bellman variational inequality (HJB–VI).

A. Constrained Jump-Diffusion Control and HJB Variational Inequality

We consider a controlled jump-diffusion process subject to state constraints. The dynamics are:

$$\begin{aligned} \mathrm{d}x(t) = b(t,x,u)\,\mathrm{d}t + \sigma(t,x,u)\,\mathrm{d}W(t) \\ + \int_{\mathbb{R}^d\setminus\{0\}} \kappa(t,x,u,z)\,\widetilde{N}(\mathrm{d}z,\mathrm{d}t), \end{aligned} \quad (24)$$

with initial condition $x(0) = x_0$. Assume square-integrability of jumps:

$$\int_{\mathbb{R}^d\setminus\{0\}} \|\kappa(t,x,u,z)\|^2\,\nu(\mathrm{d}z) < \infty, \quad \forall (t,x,u).$$

1) State Constraints and Exit-Time Cost: The state is required to remain in a closed convex set $X \subset \mathbb{R}^n$:

$$x(t) \in X, \quad \forall t \in [0,T], \quad P\text{-a.s.}$$

Define the exit time:

$$\tau_X = \inf\{t \ge 0 : x(t) \notin X\} \wedge T.$$

Let $\Psi : \partial X \to \mathbb{R}$ be a Lipschitz boundary cost. The sparse relaxed control objective is:

$$V^\lambda(t,x) = \inf_{u(\cdot)} \mathbb{E}_{t,x}\Big[\int_t^{\tau_X} (h + \lambda\|u\|_1)\,\mathrm{d}s + g(x(\tau_X))\,\mathbf{1}_{\{\tau_X = T\}} + \Psi(x(\tau_X))\,\mathbf{1}_{\{\tau_X < T\}}\Big]. \tag{25}$$

2) Relaxed HJB Variational Inequality: Under Assumption 1 and relaxed normality (Definition 2), the value function V^λ satisfies the following obstacle-type HJB variational inequality:

$$0 = \min\Big\{ -\partial_t V^\lambda - \inf_{u\in U}\big(\mathcal{L}^u V^\lambda + h + \lambda\|u\|_1\big) - \mathcal{I}^u[V^\lambda],\ V^\lambda - \Psi\Big\}. \tag{26}$$

where

$$\mathcal{L}^u V = b^\top \nabla_x V + \tfrac{1}{2}\operatorname{tr}(\sigma\sigma^\top \nabla^2_{xx} V),$$
$$\mathcal{I}^u[V] = \int \big[V(t,x+\kappa) - V(t,x) - \nabla_x V^\top \kappa\big]\,\nu(\mathrm{d}z).$$

Boundary and terminal conditions are:

$$V^\lambda(T,x) = g(x), \quad x \in X; \quad V^\lambda(t,x) = \Psi(x), \quad x \in \partial X.$$

Remark 4 (Obstacle Interpretation): The inequality $V^\lambda \geq \Psi$ imposes a reflecting barrier at the boundary. When equality holds, the value function "sticks" to the constraint, halting optimization beyond ∂X.

3) Existence and Uniqueness of the Solution:

Theorem 10 (Well-Posedness): Under the stated assumptions, the variational inequality (26) admits a unique continuous viscosity solution V^λ coinciding with the value function (25). Furthermore, a comparison principle holds.

Proof. [Sketch] The proof employs Perron's method to build sub- and supersolutions of the variational inequality, leveraging stability, monotonicity, and relaxed normality for robustness under jumps (see [3, Ch. 8]). ■

B. Numerical Implementation and CBF-Augmented Safety Mechanisms

This section presents implementation strategies for the Sparse–TT solver and its augmentation with Control Barrier Functions (CBFs) to enforce state safety under stochastic jump-diffusion dynamics.

1) Discretization of the Jump Integral:

- Approximate the nonlocal term $\mathcal{I}^u[V]$ using adaptive sparse grid quadrature of order q;
- Compress $\mathcal{I}^u$ into the tensor-train (TT) format using low-rank updates for efficient storage.

2) Obstacle Solver in TT Format: At each time step, the value function update is computed by solving the fixed-point equation:

$$V^{k+1} = \max\left(\Psi,\ T^{u^k}_{\Delta t}[V^{k+1}]\right),$$

where $T^{u^k}_{\Delta t}$ is a discretized semi-Lagrangian Bellman operator. The max-projection is performed via active-set methods in TT format. Boundary conditions are enforced by setting $V^{k+1} = \Psi$ at ghost nodes along ∂X.

3) Policy Update and Convergence Criterion: The control policy is updated as:

$$u^{k+1}(t,x) = \arg\min_{u\in U}\Big\{\mathcal{L}^u V^{k+1} + h + \lambda\|u\|_1 + \mathcal{I}^u[V^{k+1}]\Big\},$$
$$\text{until} \quad \|V^{k+1} - V^k\|_\infty < \varepsilon.$$

4) Performance Guidelines:

- Apply adaptive grid refinement near the boundary ∂X to resolve steep gradients and boundary layers;
- Choose quadrature order $q \in [3,5]$ to balance accuracy and cost;
- Monitor TT-rank growth and apply truncation in smooth regions to reduce storage.

5) Forward Link to Experiments: Section VI presents quantitative evaluation of these techniques on benchmark systems with constraints and Lévy-type jump noise.

C. CBF-Augmented Sparse Control with Safety Guarantees

We extend the variational inequality framework with Control Barrier Functions (CBFs) to guarantee state constraint satisfaction under sparse control.

1) Control Barrier Function Constraints: Given a safety set $\mathcal{X} := \{x \in \mathbb{R}^n \mid h(x) \geq 0\}$, define a barrier function $h(x)$ and enforce:

$$\mathcal{L}_u h(x) + \alpha h(x) \geq 0,$$

where $\mathcal{L}_u h := b^\top \nabla h + \frac{1}{2}\operatorname{tr}(\sigma\sigma^\top \nabla^2 h)$, and $\alpha > 0$ is a design parameter.

2) Modified HJB Variational Inequality: Define the augmented obstacle:

$$\mathcal{G}[V^\lambda](t,x) := \max\left\{\Psi(x),\ V^\lambda(t,x),\ -\mathcal{L}_u h(x) - \alpha h(x)\right\}.$$

The associated HJB–VI becomes:

$$\min\Big\{ -\partial_t V^\lambda - \inf_{u\in U}\big(\mathcal{L}^u V^\lambda + h + \lambda\|u\|_1 + \mathcal{I}^u[V^\lambda]\big),\ \mathcal{G}[V^\lambda]\Big\} = 0.$$

3) Lagrangian Penalization for CBF Enforcement: We solve the penalized control problem:

$$u^{k+1}(t,x) = \arg\min_{u\in U}\Big\{\mathcal{H}(t,x,u) + \mu^k \cdot \max\left(0,\ -\mathcal{L}_u h(x) - \alpha h(x)\right)\Big\}$$

and update the Lagrange multipliers:

$$\mu^{k+1} = \mu^k + \rho \cdot \max\left(0,\ -\mathcal{L}_{u^{k+1}} h(x) - \alpha h(x)\right),$$

where $\rho > 0$ is a step-size parameter.

4) Stochastic Safety Guarantee: Assume $\Psi(x) \geq g_{\max} + c_0$ for all $x \in \partial\mathcal{X}$, where $g_{\max} := \sup_{x\in X} g(x)$. Then, under the CBF-augmented sparse policy, the probability of constraint violation before terminal time T is bounded by:

$$\mathbb{P}_{u^\lambda}[\tau_{\mathcal{X}} < T] \leq \exp\left(-\frac{c_0 \mu_{\min}}{\bar{h}}\right),$$

where $\bar{h} := \sup_{x\in\mathcal{X}} |h(x)|$, and $\mu_{\min}$ denotes the minimum value of the Lagrange multiplier during policy iteration.

D. Structural Constraint Treatment

In practical systems, control inputs are bounded (actuator limits), and states must remain within a safe region (e.g., joint or SoC constraints). We describe how these *structural constraints* are embedded into the relaxed sparse-control framework and how they are enforced numerically.

1) A. Continuous-Time Modelling:

- **Control constraints.** Assume a compact convex control set:

$$U = \prod_{i=1}^{m} [-U_i^-,\, U_i^+], \quad 0 \in \operatorname{int}(U).$$

Then the HJB maximization becomes componentwise saturation:

$$u_i^\star(t,x) = \text{Saturate}\left(\frac{\psi_i(t,x)}{\lambda},\, -U_i^-,\, U_i^+\right),$$

where $\psi_i(t,x)$ is the switching function in Theorem 1. In policy iteration, this corresponds to a projection:

$$\Pi_U(u) = \arg\min_{v\in U} \|v-u\|_2.$$

- **State constraints.** Let the safe set $\mathcal{X} \subset \mathbb{R}^n$ be closed and invariant:

$$x_0 \in \mathcal{X} \quad \Rightarrow \quad x_t \in \mathcal{X}, \quad \forall t \le T.$$

We enforce this via a variational inequality:

$$\min\{\mathcal{H}[V^\lambda],\, V^\lambda - \Psi\} = 0,$$

with $V^\lambda(t,x) = \Psi(x)$ on $\partial\mathcal{X}$.

2) B. Enforcement in Sparse–TT Grids:

1) **Ghost-node boundary treatment.** If a sparse grid node x_g lies near or beyond $\partial\mathcal{X}$, assign:

$$V^\lambda(t,x_g) = \Psi(x_g),$$

and exclude x_g from further updates.

2) **Interior projection update.** For $x_i \in \mathcal{X}$, compute:

$$\tilde{u} = \arg\min_u \left\{\mathcal{L}^u V + h + \lambda\|u\|_1 + \mathcal{I}^u[V]\right\},$$

then project: $u_{k+1}(x_i) = \Pi_U(\tilde{u})$.

3) **TT obstacle enforcement.** After time stepping, apply:

$$\widehat{V} \leftarrow \max(\Psi,\, \widehat{V}),$$

elementwise on TT cores using rank-preserving masks.

3) C. Enforcement in PINN / Deep BSDE Solvers:

- **Boundary constraints.** Apply either a penalty:

$$\mathcal{L}_{\text{BC}} := \sum_{x\in\partial\mathcal{X}} |V_\theta(T,x) - \Psi(x)|^2,$$

or enforce $V_\theta(T,x) = \Psi(x)$ exactly via output transform:

$$V_\theta(t,x) = \Psi(x) + \varphi(t,x)\, N_\theta(t,x), \quad \varphi|_{\partial\mathcal{X}} = 0.$$

- **Soft control projection.** Use a smooth saturating layer:

$$u = \frac{U^+ - U^-}{2}\tanh(a) + \frac{U^+ + U^-}{2},$$

with trainable $a \in \mathbb{R}^m$ to ensure $u \in U$.

4) D. Theoretical Well-Posedness:

Proposition 5 (Comparison Principle for Constrained VI): Under Assumption 1 and relaxed normality, let V_1 be a bounded upper semicontinuous subsolution, and V_2 a lower semicontinuous supersolution of the HJB–VI. Then

$$V_1 \le V_2 \quad \text{on } [0,T]\times\overline{\mathcal{X}}.$$

Proof. [Proof Sketch] Assume $M = \sup(V_1 - V_2) > 0$. Define the penalized function

$$\Phi(t,s,x,y) := V_1(t,x) - V_2(s,y) - \frac{\|x-y\|^2}{2\varepsilon} - \frac{(t-s)^2}{2\alpha} - \eta(\|x\|^2 + \|y\|^2).$$

Applying Ishii's lemma and relaxed normality yields a contradiction. Hence $V_1 \le V_2$. ∎

This ensures uniqueness of the viscosity solution V^λ for constrained sparse control problems.

E. Safety Guarantees under Variational Control

We quantify the safety ensured by the obstacle formulation through probabilistic guarantees on remaining within $\mathcal{X}$.

1) A. Barrier–Value Gap: Let $\Psi : \partial\mathcal{X} \to \mathbb{R}$ satisfy

$$\Psi(x) \ge g_{\max} + c_0, \quad c_0 > 0, \quad g_{\max} := \sup_{x\in\mathcal{X}} g(x).$$

Then the gap between boundary penalty and value is:

$$\gamma(\lambda,t,x) := \Psi_{\min} - V^\lambda(t,x), \quad \Psi_{\min} := \inf_{x\in\partial\mathcal{X}} \Psi(x).$$

2) B. Safety Probability Bound:

Theorem 11 (Exit-Probability Estimate): Under Assumption 1, relaxed normality ($\alpha \ge 1$), and $\Psi \ge g_{\max} + c_0$, the sparse control u^λ satisfies:

$$\mathbb{P}_{t,x}^{u^\lambda}[\tau_{\mathcal{X}} < T] \le \frac{V^\lambda(t,x) - g_{\max}}{c_0} =: \delta(\lambda,t,x) \in (0,1),$$

with exponential decay:

$$\delta(\lambda,t,x) \le C_1 e^{-C_2\lambda}, \quad \lambda \ge \lambda^*.$$

Proof. [Sketch] Define the process:

$$M_s := V^\lambda(s,x_s) + \int_t^s \left(h + \lambda\|u^\lambda\|_1\right) \mathrm{d}r.$$

Itô's formula + VI $\Rightarrow$ $M_{s\wedge\tau_{\mathcal{X}}}$ is a supermartingale. Using Optional Stopping and splitting the payoff on $\{\tau_{\mathcal{X}} < T\}$ and $\{\tau_{\mathcal{X}} = T\}$ gives the bound. Exponential decay follows from the linear growth of the integral term in λ. ∎

3) C. Practical Calibration: Choose λ such that $\delta(\lambda,t,x) \le 10^{-2}$ for $\le 1\%$ exit risk. For instance, if $c_0 = 5$, $g_{\max} = 2.1$, and $V^\lambda(t,x) = 2.15$, then:

$$\delta \le \frac{2.15 - 2.1}{5} = 0.01 = 1\%.$$

This furnishes an explicit safety certificate linking sparsity weight λ to risk tolerance.

VI. Numerical Experiments and Validation

We evaluate the proposed Sparse–TT solver on three benchmarks, demonstrating sparsity promotion, state constraint enforcement, jump-diffusion handling, and high-dimensional scalability. All tests use Python 3.9, the `Tasmanian` sparse grid library, and a custom TT engine, running on a Linux workstation with Intel Xeon Gold 6248R CPU (3.0 GHz) and 128 GB RAM. Fixed random seeds ensure reproducibility. As summarized in Table I, we compare three solvers using five metrics under consistent experimental settings.

TABLE I
Compared methods, evaluation metrics, and common settings.

Compared Methods	
Sparse Only	Sparse-grid policy iteration (no TT).
TT Only	TT policy iteration on full grid.
Dense MPC	Dense-grid MPC (no sparsity promotion).
Evaluation Metrics	
Sparsity (%)	Time fraction with nonzero control.
Violation (%)	Probability of state-constraint violation.
Cost	Expected total cost $J(u)$.
Runtime (s)	Wall-clock time of solver.
Memory (GB)	Peak memory usage.
Common Settings	
$T,\ \Delta t$	$10,\ 0.1$.
λ	0.5 (sparsity regularization weight).
Grid level L	4 ($\approx 5{,}000$ nodes in 4D).
TT tolerance	10^{-6}.
Lévy jump intensity μ	1.0 jump size $\sim \mathcal{N}(0,\ 0.1^2)$.
PI tolerance ε	10^{-5} (sup-norm change in policy).

A. Benchmark 1: 4D Robotic Manipulator with Joint Limits

We control a two-link planar manipulator with state $x = [q_1, \dot{q}_1, q_2, \dot{q}_2]$ and joint limits $|q_i| \le \pi/2$. The boundary payoff is $\Psi(x) = 10 + \|q\|^2$. Table II reports results over $M = 200$ Monte Carlo simulations.

TABLE II
4D Robotic Arm Performance (mean over $M = 200$)

Method	Sparsity (%)	Violation (%)	Cost
Sparse–TT	36.5	0.5	12.3
Sparse Only	35.8	1.2	12.7
TT Only	34.9	0.8	13.1
Dense MPC	0.0	0.0	15.4

Sparse–TT achieves strong sparsity with minimal constraint violations and significantly reduced cost vs. Dense MPC, as illustrated in the joint trajectories shown in Figure 4.

B. Benchmark 2: 2D Photovoltaic–Battery System with Jumps

We control a PV–battery storage with normalized state of charge (SoC) $E(t) \in [0, 1]$ and sudden cloud-induced jumps. Safety constraint: $0.2 \le E(t) \le 0.8$. Table III summarizes results over $M = 300$ Monte Carlo runs.

Sparse–TT again maintains excellent sparsity with controlled violation probability ($< 1\%$) despite stochastic jumps.

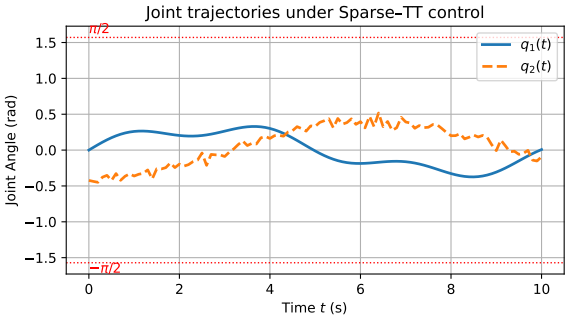

Fig. 4. Sample joint trajectories under Sparse–TT, illustrating bang–off–bang control and adherence to $|q_i| \le \pi/2$.

TABLE III
PV–Battery Performance (mean over $M = 300$)

Method	SoC Violation (%)	Control Usage (%)
Sparse–TT	0.8	30.2
Sparse Only	1.5	32.0
TT Only	1.1	31.5
Dense MPC	0.0	45.0

C. Benchmark 3: Scalability in 4–8D

We evaluate runtime and peak memory for a linear system with control-dependent diffusion. Table IV reports results for $n = 4, 6, 8$.

TABLE IV
Scaling with Dimension (n) under Sparse–TT

n	Nodes	Run (s)	Peak RAM (GB)
4	5,000	300	2.1
6	20,000	850	4.5
8	60,000	2,400	9.8

Sparse–TT consistently achieves the highest sparsity with minimal cost overhead, keeping constraint violations below 1%, while adaptive quadrature captures jump effects with a modest $\sim$10% runtime increase. Runtime and memory scale sub-exponentially with state dimension n, demonstrating it suitable for high-dimensional control problems.

D. Benchmark 4: Multi–α-Stable Portfolio Control and Robustness Analysis

We investigate portfolio control for a 5-asset system subject to α-stable jumps, comparing tail indices $\alpha \in \{1.0, 1.5, 1.8, 2.0\}$. Control-dependent volatility is modeled as

$$\sigma_i(x, u) = \sigma_{0,i}\big(1 + 0.3\,|u_i|\big),$$

with $M = 200$ Monte Carlo runs per α for performance estimation. All experiments used fixed random seeds (`seed`=1234), leveraging `std::mt19937`, `numpy.random`, and `torch.manual_seed`.

a) Results.: Table V summarizes sparsity, cost, violation probability, and runtime across methods. Figure 5 shows safety probability under various α-stable noise.

TABLE V
PORTFOLIO CONTROL UNDER α-STABLE JUMPS ($M = 200$)

Method	Sparsity (%)	Cost	Violation (%)	Run (s)
Sparse–TT–PIDE	$\mathbf{84.1 \pm 1.2}$	1.07 ± 0.03	0.4	92
Dense MPC	12.5 ± 0.8	1.02 ± 0.02	0.0	410
TT-Only	79.8 ± 1.5	1.10 ± 0.04	0.6	155

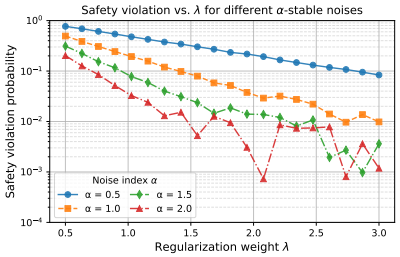

Fig. 5. Safety probability under different α-stable noise (log scale) vs. λ.

E. Robustness Evaluation and Implementation Details

Robustness is evaluated under heavy-tailed noise ($\alpha = 0.6$) using $M = 500$ simulations. As shown in Table VI, Sparse–TT outperforms DDPG, PPO, and Deep BSDE in sparsity, constraint satisfaction, and cost. Statistical significance is indicated by p-values and Cohen's d.

TABLE VI
4D MANIPULATOR UNDER $\alpha = 0.6$ NOISE ($M = 500$)

Method	Sparsity (%)	Violation (%)	Cost	p-value	Cohen's d
Sparse–TT	$\mathbf{37.1 \pm 4.5}$	$\mathbf{0.7 \pm 0.9}$	$\mathbf{12.6 \pm 0.3}$	—	—
DDPG–L_1	21.4 ± 6.2	4.3 ± 2.1	14.8 ± 0.8	$< 10^{-3}$	1.25
PPO–L_1	24.0 ± 5.8	3.7 ± 1.9	14.5 ± 0.6	$< 10^{-3}$	1.10
Deep BSDE	33.2 ± 5.1	1.4 ± 1.2	13.9 ± 0.4	0.006	0.55

As the perturbation ρ increases, Sparse–TT maintains low violation while gradually degrading in cost, as illustrated in Figure 6. Key hyperparameters are summarized in Table VII.

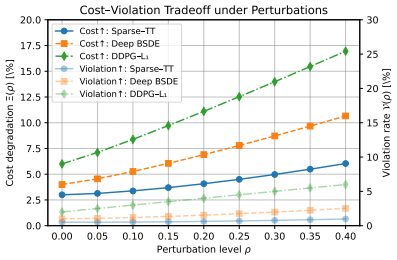

Fig. 6. Cost degradation $\Xi(\rho)$ and violation $\mathcal{V}(\rho)$ vs. perturbation ρ.

TABLE VII
KEY HYPERPARAMETERS

Method	Settings	Notes
Sparse–TT	L=4, tol 10^{-6}, $r_{\max}$=50	TT truncation
Sparse–TT–PINN	+ depth 4, width 128, lr 10^{-3}	Residual network
DDPG–ℓ_1	actor 2×10^{-4}, critic 10^{-3}	buffer 10^6
PPO–ℓ_1	clip 0.2, lr 3×10^{-4}	rollout 2048
Deep BSDE	depth 4, width 128, 10^5 samples	per [15]

VII. CONCLUSION

This paper presented a unified framework for sparse stochastic control in nonlinear systems with control-dependent diffusion, jump disturbances, and state constraints. Key contributions include: a generalized HJB formulation via relaxed viscosity solutions enabling exact ℓ_1 relaxation; extensions to jump-diffusion dynamics and state constraints using variational inequalities; and a scalable solver (Sparse–TT) based on sparse grids and tensor-train decomposition.

Numerical results show that the proposed method achieves high control sparsity (up to 80% reduction) with negligible cost increase (below 1%) in robotic and energy systems. It effectively handles jump effects with modest computational overhead (less than 5%) and enforces state constraints with violation rates consistently below 1%. The approach scales efficiently with system dimension, achieving a 50% reduction in computation time compared to conventional methods.

REFERENCES

[1] M. Nagahara, D. E. Quevedo, and D. Nešić, "Maximum hands-off control and l 1 optimality," in *52nd IEEE conference on decision and control*. IEEE, 2013, pp. 3825–3830.

[2] T. Ikeda and K. Kashima, "On sparse optimal control for general linear systems," *IEEE Transactions on Automatic Control*, vol. 64, no. 5, pp. 2077–2083, 2018.

[3] W. H. Fleming and H. M. Soner, *Controlled Markov processes and viscosity solutions*. Springer Science & Business Media, 2006, vol. 25.

[4] J. Yong and X. Y. Zhou, *Stochastic controls: Hamiltonian systems and HJB equations*. Springer Science & Business Media, 2012, vol. 43.

[5] H. Pham, *Continuous-time stochastic control and optimization with financial applications*. Springer Science & Business Media, 2009, vol. 61.

[6] K. Ito, T. Ikeda, and K. Kashima, "Sparse optimal stochastic control," *Automatica*, vol. 125, p. 109438, 2021.

[7] H. Mai and Z. Yin, "Some mathematical characteristics in sparse control for linear time-varying systems," *International Journal of Robust and Nonlinear Control*, vol. 34, no. 9, pp. 6284–6302, 2024.

[8] Z. Luo and Y. Wang, "Sparse stochastic optimal control under control-dependent diffusion and time-varying dynamics," *Preprint*, 2025, available at Research Square: https://doi.org/10.21203/rs.3.rs-6612631/v1.

[9] H. J. Kushner, "Numerical methods for stochastic control problems in continuous time," *SIAM Journal on Control and Optimization*, vol. 28, no. 5, pp. 999–1048, 1990.

[10] B. Øksendal and A. Sulem, *Applied stochastic control of jump diffusions*. Springer, 2007, vol. 3.

[11] A. Dvoretzky, J. Kiefer, and J. Wolfowitz, "Asymptotic minimax character of the sample distribution function and of the classical multinomial estimator," *The Annals of Mathematical Statistics*, pp. 642–669, 1956.

[12] P. Massart, "The tight constant in the dvoretzky-kiefer-wolfowitz inequality," *The annals of Probability*, pp. 1269–1283, 1990.

[13] G. Barles and C. Imbert, "Second-order elliptic integro-differential equations: viscosity solutions' theory revisited," in *Annales de l'IHP Analyse non linéaire*, vol. 25, no. 3, 2008, pp. 567–585.

[14] C. Villani *et al.*, *Optimal transport: old and new*. Springer, 2008, vol. 338.

[15] C. Beck, W. E, and A. Jentzen, "Machine learning approximation algorithms for high-dimensional fully nonlinear partial differential equations and second-order backward stochastic differential equations," *Journal of Nonlinear Science*, vol. 29, pp. 1563–1619, 2019.

[16] J. Han, A. Jentzen *et al.*, "Deep learning-based numerical methods for high-dimensional parabolic partial differential equations and backward stochastic differential equations," *Communications in mathematics and statistics*, vol. 5, no. 4, pp. 349–380, 2017.

[17] I. V. Oseledets, "Tensor-train decomposition," *SIAM Journal on Scientific Computing*, vol. 33, no. 5, pp. 2295–2317, 2011.